MAGNETIC RESONANCE IN CHEMISTRY
Magn. Reson. Chem. 2002; **40**: 97–106

Solid-state $^1H \rightarrow {}^{19}F/{}^{19}F \rightarrow {}^1H$ CP/MAS NMR study of poly(vinylidene fluoride)

Shinji Ando,[1] Robin K. Harris[2]* and Stefan A. Reinsberg[2†]

[1] Department of Organic and Polymeric Materials, Tokyo Institute of Technology, Ookayama, Meguro-ku, Tokyo 152-8552 Japan
[2] Department of Chemistry, University of Durham, South Road, Durham DH1 3LE, UK

Received 4 June 2001; Revised 3 August 2001; Accepted 14 September 2001

Solid-state $^1H \rightarrow {}^{19}F$ and $^{19}F \rightarrow {}^1H$ cross-polarization magic angle spinning (CP/MAS) NMR spectra have been investigated for a semicrystalline fluoropolymer, namely poly(vinylidene fluoride) (PVDF). The $^1H \rightarrow {}^{19}F$ CP/MAS spectra can be fitted by five Lorentzian functions, and the amorphous peaks were selectively observed by the DIVAM CP pulse sequences. Solid-state spin-lock experiments showed significant differences in $T_{1\rho}^{F}$ and $T_{1\rho}^{H}$ between the crystalline and amorphous domains, and the effective time constants, T_{HF}^{*} and $T_{1\rho}^{*}$, which were estimated from the $^1H \rightarrow {}^{19}F$ CP curves, also clarify the difference in the strengths of dipolar interactions. Heteronuclear dipolar oscillation behaviour is observed in both standard CP and $^1H \rightarrow {}^{19}F$ inversion recovery CP (IRCP) experiments. The inverse $^{19}F \rightarrow {}^1H$ CP-MAS and $^1H \rightarrow {}^{19}F$ CP-drain MAS experiments gave complementary information to the standard $^1H \rightarrow {}^{19}F$ CP/MAS spectra in a manner reported in our previous papers for other fluoropolymers. The value of N_F/N_H (where N is a spin density) estimated from the CP-drain curve is within experimental error equal to unity, which is consistent with the chemical structure. **Copyright © 2001 John Wiley & Sons, Ltd.**

KEYWORDS: NMR; ^{19}F NMR; ^1H NMR; fluoropolymer; poly(vinylidene fluoride); magic-angle spinning; phase structure; cross-polarization dynamics; relaxation parameter

INTRODUCTION

Poly(vinylidene fluoride) (PVDF), which has the molecular unit —(CH_2CF_2)—, is a semicrystalline polymer having a large dipole moment in the repeating unit. It exhibits interesting electric properties, such as ferroelectricity, piezoelectricity and pyroelectricity when it exists in special crystalline forms. Although five such forms have been reported, two major crystalline ones, namely the α- and β-polymorphs, frequently exist in as-polymerized powder.[1,2] The chains of the α- form have the tg^+tg^- conformation, whereas those in the β-form have the all-*trans* conformation. Although solution-state ^{19}F NMR of PVDF dissolved in dimethyl-d_6 sulfoxide has been investigated by several workers,[3–7] high-resolution solid-state NMR studies have been limited until recently because of the existence of two abundant spin baths, fluorine and hydrogen.

We have reported a series of solid-state ^{19}F, ^1H and ^{13}C NMR studies on PVDF.[8–11] Holstein *et al*.[8] reported that, with ^1H decoupling, PVDF powder obtained from the melt shows a major signal at $\delta_F = -91$ ppm, together with two shoulders at lower and higher frequencies, and a weak doublet at a significantly lower frequency ($\delta_F = -116$ and -120 ppm, uncorrected for the Bloch–Siegert effect). The doublet peaks were assigned to the two different CF_2 groups of the tail-to-tail chain imperfections (—CF_2—CH_2—CF_2^*—CF_2—CH_2—CH_2— and —CF_2—CH_2—CF_2—CF_2^*—CH_2—CH_2—), and the shoulders arise from crystalline domains. They showed that discrimination in favour of the crystalline domains can be enhanced by a long spin-locking applied to the protons prior to CP contact, because $T_{1\rho}^{H}$ is substantially shorter for amorphous chains than for the crystalline regions. On the other hand, the dipolar dephasing pulse sequence can be used to discriminate in favour of the amorphous domain. They compared the proton and fluorine relaxation times determined by spin-lock experiments and the effective parameters (T_{HF}^{*}, $T_{1\rho}^{*}$) relating to $^1H \rightarrow {}^{19}F$ CP. Scheler and Harris[9] applied the two-dimensional (^1H and ^{19}F) wideline separation (WISE) sequence to PVDF, which clarifies the mobility differences between the amorphous and crystalline domains. The signals from the crystalline and amorphous domains were clearly distinguished in the proton lineshapes and the second moments of the lines. Holstein *et al*.[10] have also shown, via partial conversion of the α-form to the β-form (by uniaxial or biaxial drawing), that the β-form gives a single signal at $\delta_F = -98$ ppm, whereas the α-form displays two resonances at $\delta_F = -82$ and -98 ppm. The immobile chains of the crystalline domains require the application of proton high-power decoupling to completely remove proton–fluorine interactions. The origin of the chemical shifts can be well

*Correspondence to: R. K. Harris, Department of Chemistry, University of Durham, South Road, Durham DH1 3LE, UK.
E-mail: r.k.harris@durham.ac.uk
†Present address: Max-Planck-Institut für Polymerforschung, Ackermannweg 10, D-55128 Mainz, Germany.
Contract/grant sponsor: UK Engineering and Physical Sciences Research Council; Contract/grant number: GR/M73514.

DOI: 10.1002/mrc.964

understood in conformational terms by the *γ-gauche* effect. Recently, Scheler[12] examined the polymorphism of PVDF by increasing the MAS rate up to 32 kHz without ^{1}H decoupling. The homo- and hetero-nuclear dipolar coupling was effectively suppressed under these conditions. The 2D spectrum, obtained using the radiofrequency-driven recoupling technique, showed that strong exchange is observed between the two signals originating from the crystalline domain, whereas the exchange between the amorphous and the crystalline domain is much weaker. Su and Tzou[13] also measured spectra using the ^{19}F fast MAS method. They reported that the two peaks assigned to the crystalline domains have different chemical shift tensors, and that their shielding anisotropies are significantly larger than that of the amorphous peak (although in their spinning sideband analysis Su and Tzou did not consider any effects of homonuclear dipolar interactions). In addition, 2D spin-diffusion experiments indicated spatial proximity between the fluorines of the two peaks assigned to the crystalline domains and between the defect structure and the amorphous domain.

In a previous study,[14] we investigated solid-state $^1\text{H} \rightarrow {}^{19}\text{F}/{}^{19}\text{F} \rightarrow {}^1\text{H}$ CP/MAS, and ^{1}H fast MAS NMR spectra of semicrystalline poly(vinyl fluoride) (PVF). The static ^{1}H pulsed NMR measurements of $T_{1\rho}^{\text{H}}$ and T_2^{H} showed two phases (immobile and mobile in nature), and a Goldman–Shen type of phase selection at 130 °C indicated that measurement of the lamellar size yields about 4.2 nm. Although the solid-state ^{19}F CP/MAS spectrum shows a featureless lineshape, the mobile region was selectively observed by a newly developed DIVAM (discrimination induced by variable-amplitude minipulses) pulse sequence. Solid-state spin-lock experiments showed significant differences in $T_{1\rho}^{\text{F}}$ and $T_{1\rho}^{\text{H}}$ between the immobile and mobile regions, and the effective ('observed') time constants, T_{HF}^* and $T_{1\rho}^*$, estimated from the $^1\text{H} \rightarrow {}^{19}\text{F}$ CP curves, also clarify the difference in the strengths of dipolar interactions.

In continuation of our work on $^1\text{H} \rightarrow {}^{19}\text{F}/{}^{19}\text{F} \rightarrow {}^1\text{H}$ CP/MAS NMR of fluoropolymers containing both fluorine and hydrogen, we report here a new investigation of spectra of PVDF in the solid state. The relationships of the directly measured parameters $T_{1\rho}^{\text{F}}$ and $T_{1\rho}^{\text{H}}$ and the observed CP parameters T_{HF}^* and $T_{1\rho}^*$ were examined for the crystalline and amorphous domains. The $^1\text{H} \rightarrow {}^{19}\text{F}$ inversion–recovery CP (IRCP) experiment was attempted in order to observe relatively weak dipolar interactions in the amorphous domain. In addition, high-resolution ^{1}H MAS NMR spectra of PVDF were investigated using the $^1\text{H} \rightarrow {}^{19}\text{F}$ CP-drain and 'inverse CP' ($^{19}\text{F} \rightarrow {}^1\text{H}$) pulse sequences.

EXPERIMENTAL

Sample

Powdered PVDF obtained from Kynar Pennwalt Chemicals was used. The sample was dried under vacuum at 110 °C for 4 h in order to evaporate absorbed water prior to being packed in the rotor.

Nuclear magnetic resonance

Solid-state MAS NMR experiments were carried out on a Chemagnetics CMX-200 spectrometer. The spectrometer operated at resonance frequencies of 188.29 MHz for fluorine and 200.13 MHz for protons. The experimental details have been reported elsewhere.[15,16] Samples were spun at the magic angle at a rate of 13.5 kHz. In general, the number of transients acquired for each spectrum was 64. The fluorine and proton r.f. fields were adjusted to fulfil the Hartmann–Hahn (H–H) condition: $|\omega_{1\text{F}}|/2\pi = |\omega_{1\text{H}}|/2\pi =$ 83 kHz. Although the signals obtained at the H–H condition were weaker than those at the sidebands, the r.f. power in the proton channel was set to the centreband prior to the experiments in order to apply the simple forms of spin-thermodynamics theory.[15] The CP experiments were carried out at ambient probe temperature. The temperature inside the rotor, which had been calibrated earlier via replacement with a sample of methanol absorbed on tetrakis(trimethylsilyl)silane at the same spinning rate,[17] was estimated to be ca 35 °C. Fluorine-19 chemical shifts are quoted with respect to the signal for $CFCl_3$ and were measured via replacement with a sample of liquid C_6F_6 (−164.3 ppm) without proton decoupling. The Bloch–Siegert effect, which is a chemical shift displacement of ca 1.4 ppm caused by the ^{1}H decoupling, was corrected after the measurements (using standardized calibrations). Proton chemical shifts are quoted with respect to the signal for $Si(CH_3)_4$ and were measured via replacement with a sample of poly(dimethylsiloxane) (0.0 ppm) without fluorine decoupling. Recycle delays of 4.5 s are sufficiently long compared with the spin–lattice relaxation time in the laboratory frame of the sample ($T_1^{\text{F}} = 0.45$ s, $T_1^{\text{H}} = 0.85$ s).

The pulse sequences for the standard variable contact time $^1\text{H} \rightarrow {}^{19}\text{F}$ CP experiment, the inversion–recovery $^1\text{H} \rightarrow {}^{19}\text{F}$ CP (IRCP) experiment, and the $^1\text{H} \rightarrow {}^{19}\text{F}$ CP-drain experiment[15] are depicted in Fig. 1(a)–(c). The IRCP experiment consists of a standard CP period with a relatively short contact time followed by a sudden phase reversal in the fluorine channel.[18] Since the spin temperature of the fluorines is inverted, the fluorine magnetization is progressively inverted during the second part of the contact time, t_{CP}, during which the signal goes through zero at a definite time. Furthermore, the CP-drain experiment is used to measure the contact time dependence of the residual ^{1}H magnetization during the $^1\text{H} \rightarrow {}^{19}\text{F}$ CP experiment. The ^{1}H magnetization is first generated by $^{19}\text{F} \rightarrow {}^1\text{H}$ CP with a standard contact time (0.5 ms). After the CP, the magnetization is retained by spin-locking for 4 ms. During this spin-lock time, the residual fluorine magnetization dephases completely. Subsequently, the fluorine spins are irradiated, and $^1\text{H} \rightarrow {}^{19}\text{F}$ CP is thus generated. The purpose of this double CP is to remove the background signal from the ^{1}H channel. The evolutions of fluorine (during CP) and proton (in the CP-drain) magnetization were observed as a function of contact time, t_{CP}, under high-resolution conditions with high-power ^{1}H and ^{19}F decoupling in the two experiments, respectively. The magnitude of the decoupling power was equivalent to about 75 kHz in this study.

A pulse sequence that can selectively observe signals having relatively long T_2^{H} is shown in Fig. 1(d). We called this pulse technique 'discrimination induced by variable-amplitude minipulses' (DIVAM). The action of this

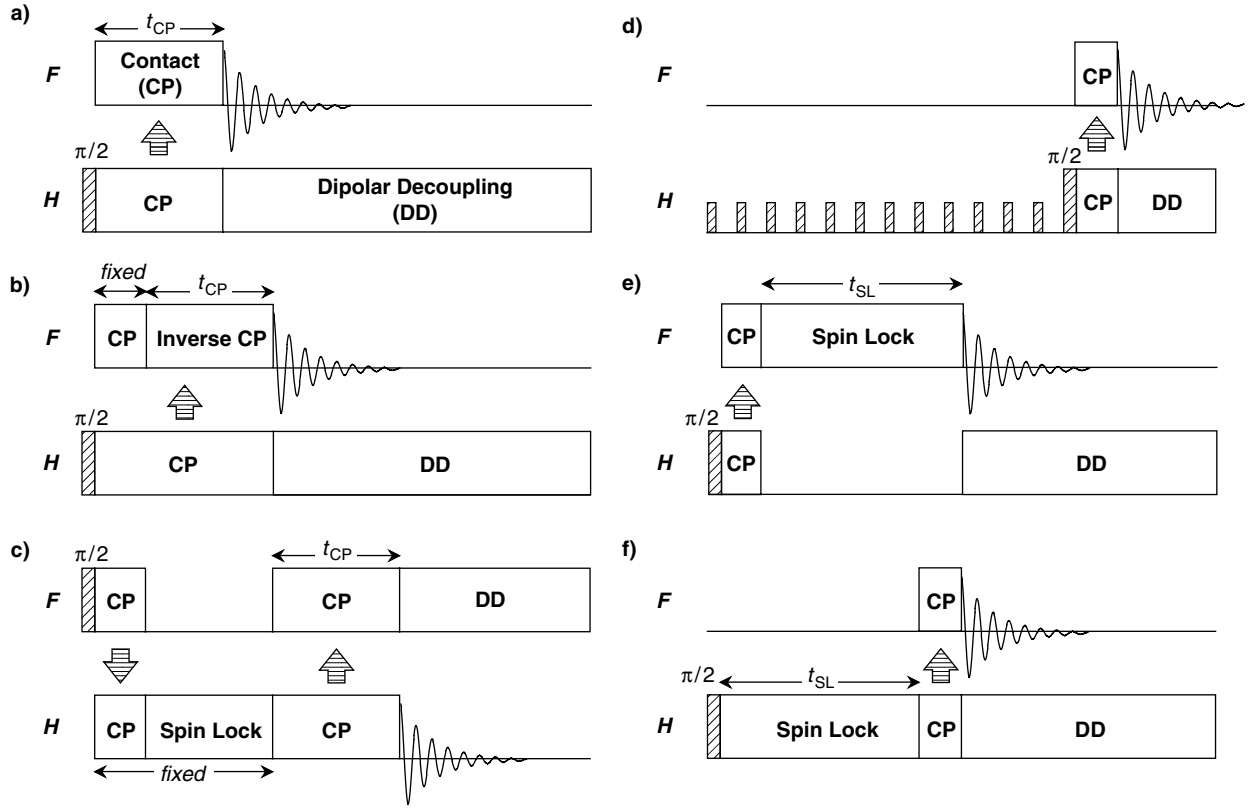

Figure 1. Pulse sequences for (a) standard variable contact-time $^1H \rightarrow {}^{19}F$ CP, (b) variable contact-time $^1H \rightarrow {}^{19}F$ inversion–recovery CP (IRCP), (c) variable contact-time CP-drain, (d) selective observation of a domain having a relatively long T_2^H (DIVAM), (e) a short-contact CP followed by variable-time ^{19}F spin-lock and (f) variable-time ^1H spin-lock followed by a short-contact CP.

pulse sequence is explained elsewhere.[14] The spin–lattice relaxation times in the rotating frame for the ^{19}F ($T_{1\rho}^F$) and ^1H ($T_{1\rho}^H$) spins were measured by variable spin-lock time experiments. The relevant pulse sequences are depicted in Fig. 1(e) and 1(f).

In the $T_{1\rho}^F$ measurement, the initial ^{19}F magnetization is generated by CP from ^1H with a short contact time (0.1 ms) and then spin-locked for a variable spin-lock time, t_{SL}. In the $T_{1\rho}^H$ measurement, the ^1H magnetization is spin-locked for a variable t_{SL} and then transferred to ^{19}F by CP for 0.1 ms. The short contact time of 0.1 ms was used to enhance the magnetization of fluorines closely attached to the spin-locked protons. As a further advantage, the dual-channel CP approach suppresses any background signals from the probe in both the ^{19}F and ^1H channels. All the pulse sequences used [except that in Fig. 1(c)] retain the advantage of the potentially greater resolution in the fluorine spectrum. The r.f. field strengths used for the spin-lock of ^1H and ^{19}F spins were kept at the same values as used for CP (i.e. equivalent to about 83 kHz). The free induction decays (FIDs) were acquired with high-power ^1H (or ^{19}F) decoupling.

RESULTS AND DISCUSSION

Selective observation of the amorphous component

Figures 2(a) and 2(b) show the ^{19}F spectra of solid PVDF powder using the $^1H \rightarrow {}^{19}F$ CP (with a contact time $t_{CP} = 0.3$ ms) and DIVAM pulse sequences[14] obtained at a spin rate of 13.5 kHz with high-power ^1H decoupling. These spectra can be fitted by combinations of five and three Lorentzian functions, respectively, as shown in Figs 2(c) and 2(d). Since the DIVAM pulse sequence selects signals from mobile domains, the major peak at $\delta_F = -92.0$ ppm (designated by open circles) and a weak doublet at lower frequency (open squares and diamonds, $\delta_F = -113.9$ and -116.2 ppm) are assigned to amorphous domains. The DIVAM spectrum also indicates that the regio-irregular units (giving the weak doublet) predominantly exist in the amorphous domains. On the other hand, the two shoulders resonating on the high- and low-frequency sides of the major amorphous signal (filled triangle and circle, $\delta_F = -82.9$ and -97.5 ppm) are assigned to crystalline domains, as was reported by Holstein and co-workers.[8,10] These signals are completely suppressed in the DIVAM spectrum.

$T_{1\rho}^F$ and $T_{1\rho}^H$ measurements

The decays of ^{19}F magnetization observed by the variable ^{19}F spin-lock experiment are shown in Fig. 3(a) as a function of the spin-lock time, t_{SL}. These plots were obtained from a series of spectra with varying t_{SL}, which were decomposed into five Lorentzian functions whose chemical shifts and widths at half-height were fixed to those derived from Fig. 2(c). The decays of ^{19}F magnetization observed in the experiment with variable ^1H spin-lock time followed by $^1H \rightarrow {}^{19}F$ CP (0.2 ms) are shown in Fig. 3(b) in the same manner as for Fig. 3(a). The directly measured $T_{1\rho}^F$ and

MRC

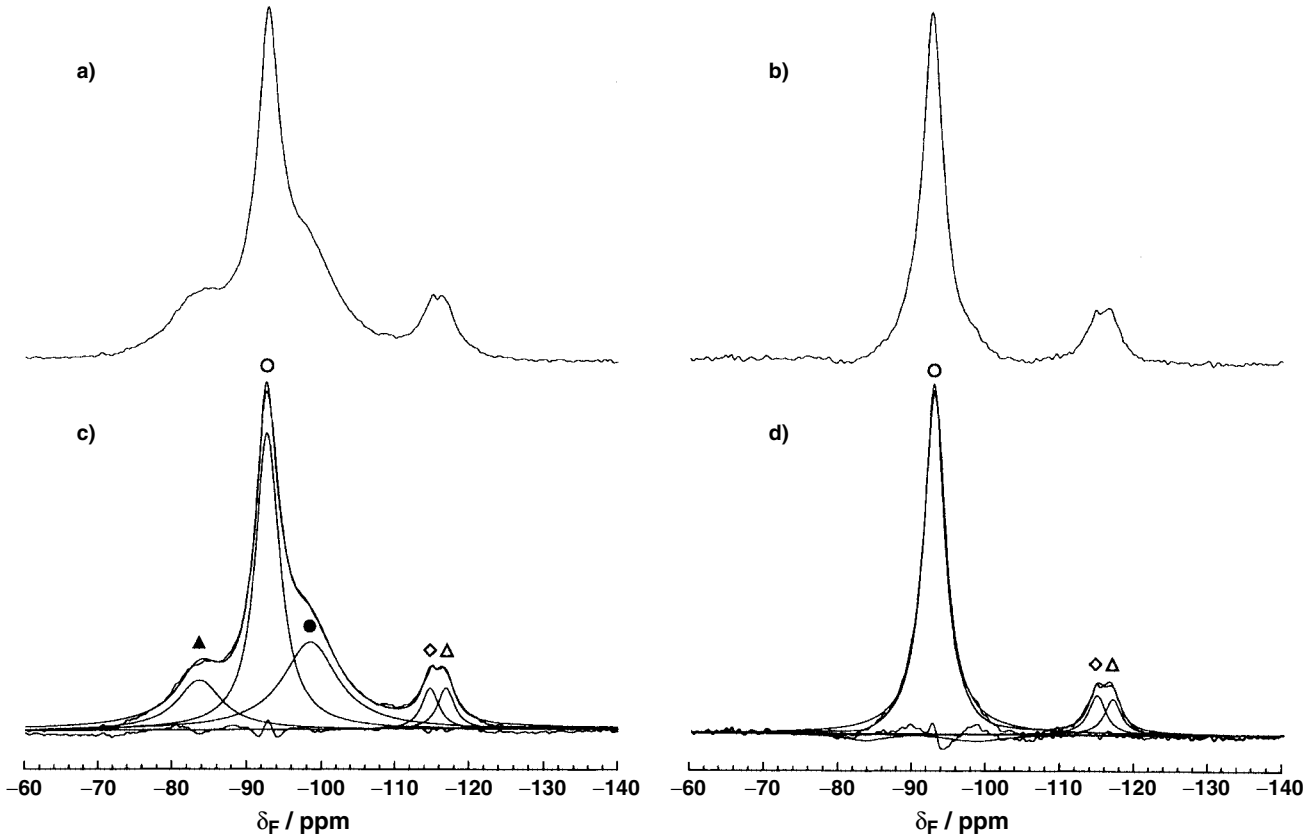

Figure 2. ^{19}F NMR spectra of PVDF: (a) ^{1}H → ^{19}F CPMAS with a contact time of 0.5 ms and (b) DIVAM spectra with ^{1}H decoupling at a spin rate of 13.5 kHz. The ^{1}H decoupling r.f. field during acquisition is equivalent to about 75 kHz. (c) The spectral decomposition of (a) using five Lorentzian functions and (d) that of (b) using three Lorentzian functions.

the indirectly measured $T_{1\rho}^{H}$ (via ^{19}F), which were obtained by fitting the decays using single or double exponential functions, are summarized in Table 1. Although the same experiments have been carried out earlier,[8] many more points of t_{SL} were taken in our study in order to obtain precise fittings. The decays of the crystalline peaks (filled symbols) have very long $T_{1\rho}^{F}$ (80–120 ms) components [Fig. 3(a)]. This agrees well with the fact that the magnetization of the crystalline domain is retained after a long spin-lock time (40 ms), whereas that of the amorphous domain is completely relaxed.[8] The short $T_{1\rho}^{F}$ component (5.2 ms) observed for the peak at −97.5 ppm (filled circle) may be caused by overlap with the major amorphous signal.

Ferguson and Brame[3] have reported, from solution-state NMR, that the CF_2 fluorines in head-to-head (CF_2—CH_2—CF_2^*—CH_2—CH_2—) sequences, which should be located in the amorphous domain, resonate at lower frequency by 3.2 ppm from the head-to-tail sequence (the major signal). This head-to-head signal may be responsible for the short-decaying component of the signal resonating at −97.5 ppm. On the other hand, the ^{19}F spin-lock decays of the amorphous peaks (open symbols) consist of short (1.3–2.9 ms) and long (8.6–10.2 ms) components. These two components have almost the same proportions. In a similar way, the spin-lock decays of the amorphous peaks consist of short (5.4–5.8 ms) and long (14.1–17.4 ms) components for the proton spin-lock experiment [Fig. 3(b)]. However, the existence of the longer relaxing component in both experiments does not necessarily indicate a two-phase nature of the amorphous domain. The influence of proton-to-proton and fluorine-to-fluorine spin diffusion between the crystalline and amorphous domains has to be considered. Holstein *et al.*[19] carried out a series of fluorine-detected proton-to-proton spin-diffusion experiments for PVDF, and they reported that the characteristic times for the crystalline → amorphous spin diffusion is 5.7–8.6 ms and that for the amorphous → crystalline spin diffusion is 4.8–5.9 ms. Although the fluorine-to-fluorine spin-diffusion time constants have never been observed for PVDF, the influence of fluorine spin diffusion is presumably of the same order but reduced by the smaller dipolar fluorine–fluorine interaction by a factor of $(\gamma_F/\gamma_H)^2$ compared with proton spin diffusion under identical conditions. In the present experiment, although the magnitude of homonuclear dipolar interactions are scaled by $-\frac{1}{2}$ under the spin-lock condition, fluorine and proton spin diffusion between the two domains should become significant after a long spin-lock time of both nuclei. Hence we consider that the longer components of $T_{1\rho}^{F}$ and $T_{1\rho}^{H}$ observed for the amorphous peaks originate from the magnetization diffused from the crystalline domain, and the inherent values of $T_{1\rho}^{F}$ and $T_{1\rho}^{H}$ can be taken from the slope at the spin-lock times shorter than 10 ms.

The large difference in $T_{1\rho}^{F}$ between the two domains, which is more than one order of magnitude, suggests that there is little or no molecular mobility in the crystalline domain at around the spin-locking frequency (several tens

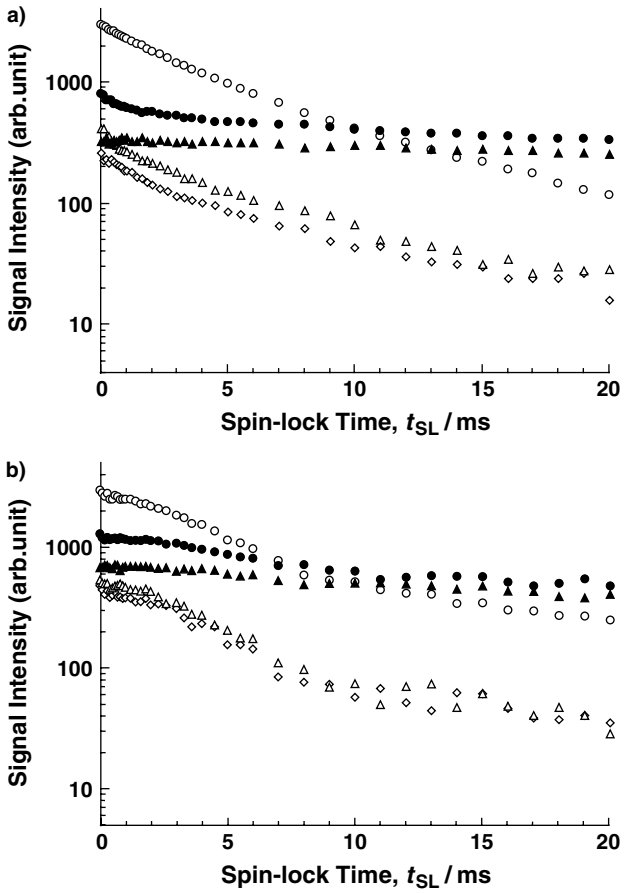

Figure 3. Spin-lock time dependence of the ^{19}F signal intensity for PVDF for (a) $^{1}H \rightarrow {}^{19}F$ CP followed by ^{19}F spin-lock and (b) ^{1}H spin-lock followed by $^{1}H \rightarrow {}^{19}F$ CP. The open and filled symbols correspond to the peaks in Fig. 2. The directly measured $T_{1\rho}^{F}$ and indirectly measured $T_{1\rho}^{H}$, obtained using single- or double-exponential functions, are summarized in Table 1.

of kHz), whereas significant molecular motion occurs in the amorphous domain. This can be supported by the fact that the melting temperature (170 °C) is much higher than the ambient probe temperature,[20] but the glass-transition temperature (−38 °C) is much lower.[21] It should be noted that the difference in the values of $T_{1\rho}^{F}$ between the two phases in PVDF is much larger than that observed for PVF.[14] This can be ascribed to the smaller content of regio-irregular structure in PVDF (5%, from solid-state ^{19}F NMR data[8]) compared with that of PVF (10.6%, from solution-state ^{13}C NMR data[22]). As clarified in Fig. 2, the content of regio-irregular sequences in the crystalline domain of PVDF is negligible, while an x-ray diffraction study reported that the crystalline domain of PVF contains ca 20% head-to-head sequence.[23]

$^{1}H \rightarrow {}^{19}F$ CP/MAS measurements

The evolutions of the ^{19}F magnetizations obtained from the standard $^{1}H \rightarrow {}^{19}F$ CP experiments are shown in Fig. 4(a) as functions of the contact time, t_{CP}. The CP curves of the amorphous peaks can be fitted by a triple-exponential function of the form

$$M(t) = -A\exp\left(-\frac{t_{CP}}{T_{HF}^{*}}\right) + \left[(A-B)\exp\left(-\frac{t_{CP}}{T_{1\rho}^{*1}}\right) + B\exp\left(-\frac{t_{CP}}{T_{1\rho}^{*2}}\right)\right] \quad (1)$$

where T_{HF}^{*}, $T_{1\rho}^{*1}$ and $T_{1\rho}^{*2}$ are effective parameters that characterize the increase and the decrease at shorter and longer t_{CP} of fluorine magnetization (the HF in T_{HF}^{*} indicates that the polarization is transferred from proton to fluorine), and A and B are fitting parameters for the signal intensity. This indicates that the increase and the decrease of magnetization can be expressed by single- and double-exponential behaviour, respectively. On the other hand, the conventional double-exponential Eqn (2) was used for the CP contact-time curves of the crystalline peaks because double-decaying components were not found:

$$M(t) = A\left[\exp\left(-\frac{t_{CP}}{T_{HF}^{*}}\right) + \exp\left(-\frac{t_{CP}}{T_{1\rho}^{*}}\right)\right] \quad (2)$$

The effective time constants determined from the fitting of the experimental curves are summarized in Table 1.

Table 1. The spin–lattice relaxation in the rotating frame and the cross-polarization parameters of each spectral component in the ^{19}F spectra (Fig. 2) of PVDF, determined from the variable spin-lock time and the variable contact time experiments (units: ms): the column headed T_{HF} lists the true values of H → F cross-polarization time constants determined from theory based on the spin-temperature hypothesis[15]

Symbol	Chemical shift (ppm)	$T_{1\rho}^{F}$	$T_{1\rho}^{H}$	T_{HF}^{*}	$T_{1\rho}^{*}$	T_{HF}	Nature
▲	−82.9	80 (100%)	32 (100%)	0.035	28 (100%)	0.07	Crystalline
○	−92.0	2.9 (58%)	5.8 (68%)	0.24	5.2 (69%)	0.51	Amorphous
		8.6 (42%)	14.1 (32%)		13.8 (31%)		
●	−97.5	5.2 (52%)	18.0 (100%)	0.057	17 (100%)	0.11	Crystalline[a]
		120 (48%)					
◊	−113.9	1.8 (50%)	5.4 (72%)	0.16	4.9 (58%)	0.32	Amorphous
		10.2 (50%)	17.4 (28%)		10.8 (42%)		
△	−116.2	1.3 (51%)	5.7 (75%)	0.12	6.2 (50%)	0.26	Amorphous
		10.0 (49%)	16.5 (25%)		13.8 (50%)		

[a] This peak is overlapped by a contribution from the amorphous region.

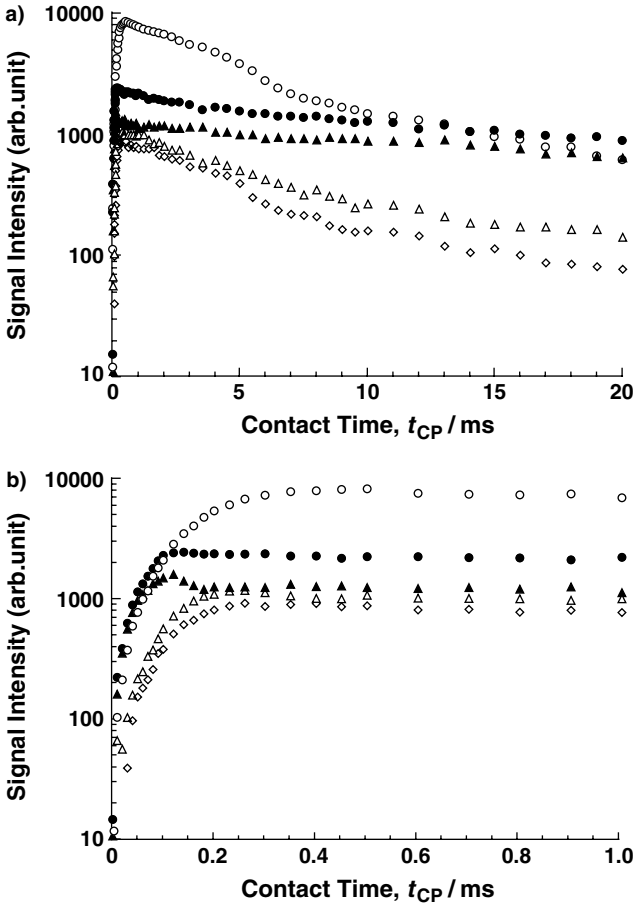

Figure 4. (a) Contact-time dependence of the ^{19}F signal intensity for the $^{1}H \rightarrow {}^{19}F$ CP experiment on PVDF and (b) its magnification for short contact times to show the dipolar oscillation behaviour.

The existence of the two decaying components in the CP curves for the amorphous peaks is straightforwardly related to the double-exponential decays in the $T_{1\rho}^{F}$ and $T_{1\rho}^{H}$ measurements, which we believe were caused by spin diffusion from the crystalline to the amorphous domain. The peaks of the crystalline domain (filled symbols) exhibit significantly shorter T_{HF}^{*} (0.035–0.057 ms) and longer $T_{1\rho}^{*}$ (17–28 ms) than those of the amorphous domain (0.12–0.24 ms for T_{HF}^{*} and 4.9–13.8 ms for $T_{1\rho}^{*}$). The shorter T_{HF}^{*} indicates that cross-polarization occurs more effectively in the crystalline domain because of the strong heteronuclear dipolar interactions. Moreover, the long $T_{1\rho}^{*}$ is also indicative of strong dipolar interactions. Since the $T_{1\rho}^{F}$ and $T_{1\rho}^{H}$ relaxation processes are comparable in efficiency, and the ratio of the number of F spins to H spins is unity in PVDF, there is no simple method to infer the true values of T_{HF} and $T_{1\rho}^{H}$ from the effective values, T_{HF}^{*} and $T_{1\rho}^{*}$. However, we have recently examined the characteristic features of CP dynamics between ^{19}F and ^{1}H in a fluorinated polyimide using $^{1}H \rightarrow {}^{19}F$ CP/MAS NMR.[15] The analysis is based on the phenomenological approach for the spin thermodynamics between two spin baths, but the high abundance of fluorine atoms and efficient $T_{1\rho}^{F}$ process were explicitly considered.

One can investigate relationships between T_{HF}^{*}, T_{HF}, $T_{1\rho}^{*}$ and $T_{1\rho}^{H}$ by introducing two parameters, f_1 and f_2:

$$T_{HF}^{*} = \frac{T_{HF}}{a_0 + \sqrt{a_0^2 - b}} = f_1 T_{HF} \tag{3}$$

$$T_{1\rho}^{*} = \frac{1}{a_0 - \sqrt{a_0^2 - b}} \frac{T_{HF}}{T_{1\rho}^{H}} T_{1\rho}^{H} = f_2 T_{1\rho}^{H} \tag{4}$$

where

$$a_0 = \frac{1}{2}\left(1 + \varepsilon + \frac{T_{HF}}{T_{1\rho}^{H}} + \frac{T_{HF}}{T_{1\rho}^{F}}\right) \tag{5}$$

and

$$b = \frac{T_{HF}}{T_{1\rho}^{H}}\left(1 + \frac{T_{HF}}{T_{1\rho}^{F}}\right) + \varepsilon \frac{T_{HF}}{T_{1\rho}^{F}} \tag{6}$$

The values of f_1 and f_2 can be calculated as functions of three parameters, namely ε, $T_{HF}/T_{1\rho}^{H}$ and $T_{HF}/T_{1\rho}^{F}$. From the definition, the value of ε is equal to unity for PVDF under the H–H condition, and the value of f_2 can be straightforwardly calculated from the directly measured values of $T_{1\rho}^{*}$ and $T_{1\rho}^{H}$ [Eqn (4)]. On the other hand, the value of f_1 for this sample is expected to be 0.45–0.5 from the contour map of f_1 calculated for the case of $\varepsilon = 1$ [Fig. 14(a) in Ref. 15]. Since the true value of T_{HF} should be significantly smaller than $T_{1\rho}^{F}$ and $T_{1\rho}^{H}$ for PVDF, T_{HF} can be determined by solving Eqn (3) by inserting the values of T_{HF}^{*}, $T_{1\rho}^{F}$, $T_{1\rho}^{H}$ and ε into the equation using numerical analysis software (e.g. Mathematica). The true values of T_{HF} thus obtained are summarized in Table 1. The smaller components of $T_{1\rho}^{F}$ and $T_{1\rho}^{H}$ are used for the calculations of the amorphous peaks because the longer components should be significantly influenced by the spin diffusion. When CP behaviour at longer values of t_{CP} is analysed, mutual exchange of magnetization between the multiple spin baths should be considered. The spin-temperature approach described above was recently generalized for any number of spin baths (Harris, Hazendonk and Pizzanelli, to be published). Typically, at modest MAS rates, a single proton spin bath but several fluorine spin baths will exist. This situation occurs when the proton spectrum is homogeneous whereas the relatively large chemical shift differences for ^{19}F ensure that separate signals are observed when proton decoupling is employed. However, there are, at least, two proton spin baths (the crystalline and amorphous domains) and five fluorine spin baths in the present system.

As shown in Table 1, the values of T_{HF} are almost twice as large as the effective value of T_{HF}^{*}, which coincides well with the prediction of the theory,[15] and indicates that the magnetization transfer from protons to fluorines occurs much faster than the conventional CP case (from an abundant spin to a rare spin). The value of T_{HF} for the major amorphous peak (−92.0 ppm) is 4.6–7.3 times longer than those of the crystalline components, which agrees well with the weaker heteronuclear dipolar interactions in the amorphous domain. It is noteworthy that the values of T_{HF} for the regio-irregular structures (resonating at lower frequencies) are slightly smaller than that of the major amorphous peak. This indicates that the heteronuclear magnetization transfer is

more efficient at tail-to-tail sequence than in the amorphous domain.

Since the polarization transfer inherently includes a coherent process, a two-stage feature is frequently detected in the initial period of cross-polarization, when there is a strongly coupled H–X spin pair.[14,24–26] The first stage originates from coherent energy transfer between directly bonded H and X spins, causing dipolar oscillations. In the second stage, an equilibration of magnetization occurs within the H spin bath via homonuclear spin diffusion. As seen in the magnification of the initial stage of $^{1}H \rightarrow {}^{19}F$ CP [Fig. 4(b)], dipolar oscillation is observed for the crystalline peak at −82.9 ppm (solid triangles), the first maximum being at 0.125 ms and the first dip at 0.225 ms. This fact indicates that there is a strongly coupled H–F spin pair in the crystalline domain, but the heteronuclear dipolar interactions are substantially reduced in the amorphous domain by motional averaging. The fact that no clear oscillation is observed for the other crystalline peak (solid circles) can be ascribed to the overlap of the amorphous signal as described above. We have analysed the transient oscillations observed in the $^{1}H \rightarrow {}^{13}C$ CP curve of poly(trifluoroethylene) (PTrFE)[27] and in the $^{1}H \rightarrow {}^{19}F$ curve of poly(vinyl fluoride)[14] in terms of interatomic distances and molecular-level mobility. However, such a detailed treatment is not feasible in the present case because the spin system involved is more complex and our data are for centreband H–H matching (in contrast to Ref. 24). On the other hand, our observations are consistent with a relative lack of motional averaging for dipolar interactions in the crystalline phase of PVDF at ambient probe temperature.

Figure 5 shows the evolutions of ^{19}F magnetization obtained from the $^{1}H \rightarrow {}^{19}F$ IRCP experiments as functions of t_{CP}. The points of the crystalline peaks (filled symbols) are translated downwards to show the oscillating behaviours clearly. The dips observed in the IRCP curves are marked by arrows. Although there is no difference in the spin dynamics between the CP and IRCP experiments, IRCP is superior to the standard CP in observing details of the initial cross-polarization processes. The dipolar oscillations are clearly observed in the initial stage, not only for the crystalline peaks, but also for the amorphous and regio-irregular peaks. The first dips are observed at 0.125 ms for the two crystalline signals, while those for the amorphous and the regio-irregular signals are observed at 0.425 and around 0.25 ms, respectively. The relatively long value may be straightforwardly ascribed to substantial molecular motion in the amorphous domains. In addition, the fact that the oscillations for the amorphous domain are weaker than for the regio-irregular sequence indicates that the former has more vigorous molecular motion than the latter. This coincides with the relatively shorter T_{HF} observed for the regio-irregular peaks than that of the major amorphous peak. It may imply that the imperfections are present in higher concentrations in areas of amorphous domains near boundaries with crystalline domains (as might be expected, since the crystallization process may be halted at imperfections).

The initial CP oscillations are not, of course, taken into account explicitly in our analysis of CP dynamics via Eqns (1)–(6). However, the oscillations only occur at short contact times for the crystalline components, whilst the spin-temperature hypothesis becomes valid at longer times. Consequently, whereas the crystalline peaks are not well fitted to Eqn (1) at short times (especially near the highest intensity), the analysis in general proceeds well and the derived parameters have significance.

$^{19}F \rightarrow {}^{1}H$ CP/MAS measurements

Figure 6 shows a $^{19}F \rightarrow {}^{1}H$ CP/MAS spectrum of PVDF with ^{19}F decoupling. No background signals are observed in the ^{1}H channel by virtue of the use of CP. The spinning sidebands originate from residual dipolar interactions which are not fully averaged by MAS at a spin rate of 13.5 kHz. Although the main peak and the spinning sidebands can

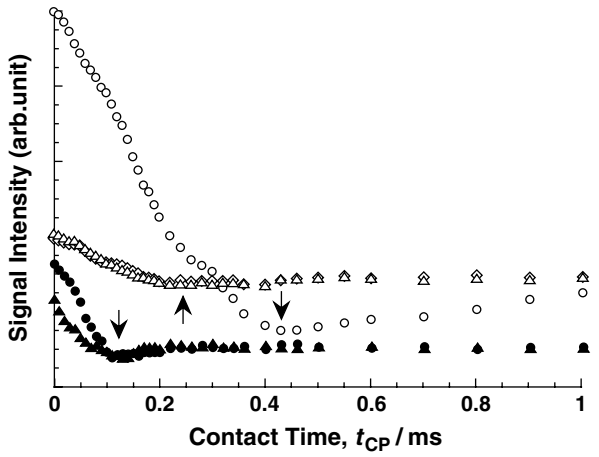

Figure 5. Contact-time dependence of the ^{19}F signal intensity for the $^{1}H \rightarrow {}^{19}F$ inversion–recovery CP (IRCP) experiment on PVDF. Dipolar oscillation behaviour is observed not only for the immobile domain but also for the mobile domain. The dips of the dipolar oscillation for the amorphous domain are observed at longer contact times than that of the crystalline domain.

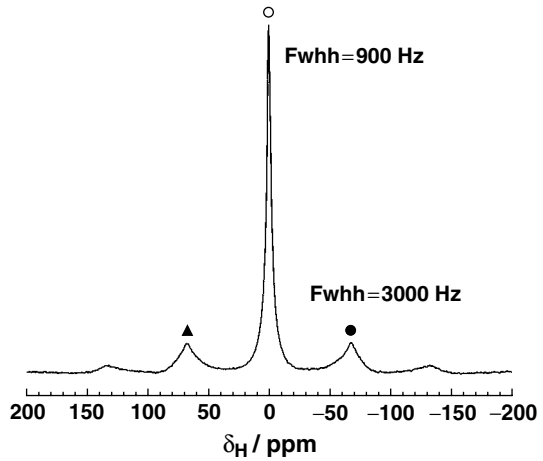

Figure 6. Solid-state $^{19}F \rightarrow {}^{1}H$ CPMAS spectrum of PVDF, obtained with a contact time of 0.5 ms. The spinning sidebands (marked by filled symbols) that originate from the residual dipolar interaction are not averaged out by the MAS at the spin rate of 13.5 kHz.

be fitted by single Lorentzian functions, the full width at half-height (FWHH) of the former (900 Hz) is significantly smaller than those of the latter (3000 Hz). This is consistent with the suggestion that the amorphous domain, in which the homonuclear dipolar interactions are significantly averaged, contributes to a relatively greater extent to the main peak than to the sidebands, as expected, though there are other possible explanations[28] for some linewidth differences between centreband and sidebands.

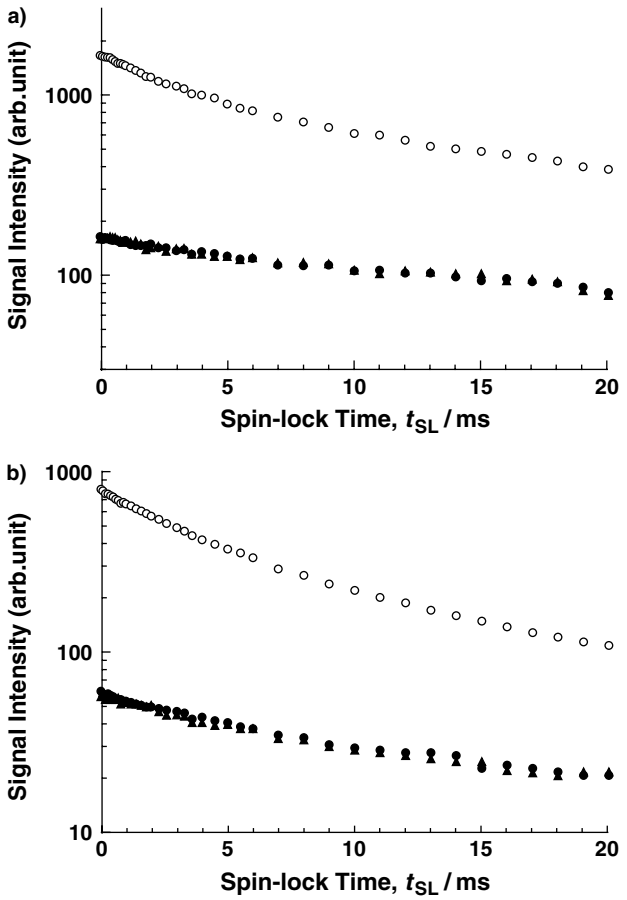

Figure 7. Spin-lock time dependence of the ^{1}H signal intensity for PVDF for (a) ^{19}F spin-lock followed by ^{19}F → ^{1}H CP and (b) ^{19}F → ^{1}H CP followed by ^{1}H spin-lock. The open and filled symbols correspond to the peaks in Fig. 6. The indirectly measured $T_{1\rho}^{F}$ and directly measured $T_{1\rho}^{H}$, obtained using single- or double-exponential functions, are summarized in Table 2.

The decays of ^{1}H magnetization observed in the experiment with variable ^{19}F spin-lock time followed by ^{19}F → ^{1}H CP (0.2 ms) as a function of t_{SL} are shown in Fig. 7(a). The open and filled symbols correspond to those in Fig. 6. A double-exponential function is required for the fitting of the main peak, whereas single-exponential functions are applicable for the sidebands. The decays of ^{1}H magnetization observed in the experiment with variable ^{1}H spin-lock time are shown in Fig. 7(b) in the same manner as for Fig. 7(a). The initial ^{1}H magnetization was generated by ^{19}F → ^{1}H CP (0.2 ms) in this experiment. The relaxation decays of the sidebands in Fig. 7(b) cannot be accurately fitted by a single exponential, but it is not easy to apply double-exponential fitting due to the small difference between the short and the long relaxation times. The indirectly measured $T_{1\rho}^{F}$ (via ^{1}H resonance) and the directly measured $T_{1\rho}^{H}$ thus obtained are summarized in Table 2. For both experiments, the main peak includes 55–60% of a short-decaying component, and the values of $T_{1\rho}^{F}$ and $T_{1\rho}^{H}$ (4.2 and 3.6 ms) are similar to those of the amorphous domain measured from the ^{19}F spectra (1.3–2.9 ms for $T_{1\rho}^{F}$ and 5.4–5.8 ms for $T_{1\rho}^{H}$). On the other hand, the sidebands in the ^{1}H spectra do not have such a short-decaying component, and the values of $T_{1\rho}^{F}$ (29 ms) and $T_{1\rho}^{H}$ (16.5 ms) are similar to those of the long-decaying component of the main peak (42.0 and 16.5 ms). These values are of the same order of magnitude as those of the crystalline domain measured from the ^{19}F spectra (80–120 ms for $T_{1\rho}^{F}$ and 18–32 ms for $T_{1\rho}^{H}$). These facts also support the assumption stated above: the amorphous domain makes little contribution to the sidebands. Holstein *et al.*[19] pointed out that, correspondingly, the spinning sidebands in a ^{1}H-decoupled ^{19}F MAS spectrum at a spin rate of 12 kHz are dominated by the spectrum of the crystalline part. Similar observations have been made by Su and Tzou.[13] Since the homonuclear dipolar interactions of hydrogens and fluorines are of the same order, the molecular motion in the amorphous domain is sufficiently vigorous as to significantly reduce the homonuclear dipolar interactions, resulting in the spinning sidebands being very weak in both ^{1}H-decoupled ^{19}F spectra and ^{19}F-decoupled ^{1}H spectra.

Figure 8 shows the evolution of the peak heights in the ^{19}F → ^{1}H CP/MAS spectra as a function of t_{CP}. For the sidebands (filled symbols), the influence of dipolar oscillation in inducing a maximum at 0.125 ms and a small dip at 0.25 ms is observed, whereas no such phenomena are observed for the main peak. On the other hand, the maximum signal intensity is observed around 0.4 ms for the main peak. In

Table 2. The spin–lattice relaxation in the rotating frame and the cross-polarization parameters of each spectral component in the ^{1}H spectra (Fig. 6) of PVDF determined from the variable spin-lock time and the variable contact time (standard CP and CP-drain) experiments (units: ms)

Symbol	Chemical shift (ppm)	Spin-lock experiment		Standard CP		CP drain		Nature
		$T_{1\rho}^{F}$	$T_{1\rho}^{H}$	T_{FH}^{*}	$T_{1\rho}^{*}$	T_{HF}^{*}	$T_{1\rho}^{*}$	
◦	2.7	4.2 (60%) 42 (40%)	3.6 (55%) 16.5 (45%)	0.23	11.7	0.090	13.5	Crystalline and amorphous
●, ▲	70.2 −64.8	29	16.5	0.07	14.0	0.043	14.7	Crystalline

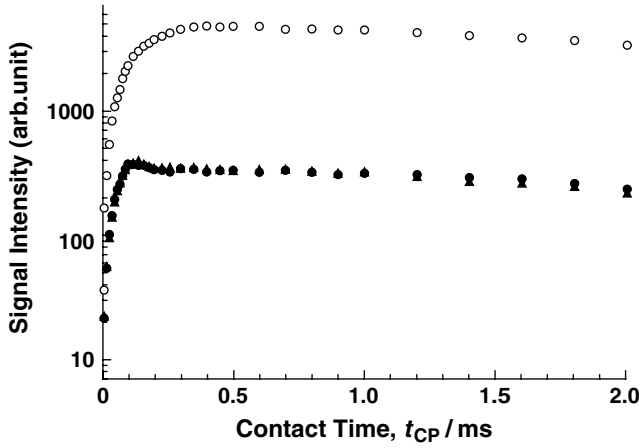

Figure 8. (a) Contact-time dependence of the ^{1}H signal intensity for the $^{19}F \rightarrow {}^{1}H$ CP experiment on PVDF and (b) its magnification for short contact times to show the dipolar oscillation behaviour. The dipolar oscillation is observed only for the spinning sidebands. The oscillation frequency is estimated as 4.0 kHz.

the crystalline domain, ^{19}F magnetization rapidly transfers to protons, but such transfer does not occur so quickly for the amorphous domain. The apparent dipolar oscillation frequency observed for the sidebands (4 kHz) coincides well with that seen for the crystalline domain in the $^{1}H \rightarrow {}^{19}F$ IRCP experiment. In addition, the maximum of the peak intensity for the main peak coincides well with the first dip observed for the amorphous peak in the $^{1}H \rightarrow {}^{19}F$ IRCP experiment. These facts clearly indicate that, for the case of PVDF, $^{19}F \rightarrow {}^{1}H$ CP/MAS NMR can give complementary information to the $^{1}H \rightarrow {}^{19}F$ CP/MAS experiments.

$^{1}H \rightarrow {}^{19}F$ CP-drain experiment

The evolution of residual ^{1}H magnetization after $^{1}H \rightarrow {}^{19}F$ CP can be monitored by the 'CP-drain' experiment which was developed by the authors.[15] The spectral shape of the residual proton signal after $^{1}H \rightarrow {}^{19}F$ CP is the same as that of the $^{19}F \rightarrow {}^{1}H$ CP spectrum, and thus the main peak and the spinning sidebands were fitted by single Lorentzian functions. Figure 9 shows the evolution of the ^{1}H magnetization obtained from the $^{1}H \rightarrow {}^{19}F$ CP-drain MAS spectra as a function of t_{CP}. Although this CP-drain curve can be fitted by a double-exponential function as predicted by theory,[15] a distinct oscillation was observed for the sidebands in the fast decaying stage. The first dip is seen at 0.125 ms, which is the same position as was observed in the $^{19}F \rightarrow {}^{1}H$ CP curve. The effective parameters obtained are $(T^{*}_{HF}, T^{*}_{1\rho}) = (0.09, 13.5\ \text{ms})$ for the main peak and (0.043, 14.7 ms) for the sidebands. As expected from the theory, the decay rate of the first step ($t_{CP} < 0.2$ ms) of the residual proton magnetization in the CP-drain curve coincides with that of the initial increase in fluorine magnetization in the $^{1}H \rightarrow {}^{19}F$ CP curve (0.035–0.24 ms; see Table 1). In addition, it has been shown that, when the H–H condition is fulfilled, the intercept of the CP-drain curve at $t_{CP} = 0$ is equal to the inverse of $(1 + N_F/N_H)$ (N being the number of spins in unit volume), if it is assumed that $T_{HF}/T^{H}_{1\rho}$ and $T_{HF}/T^{F}_{1\rho}$ are

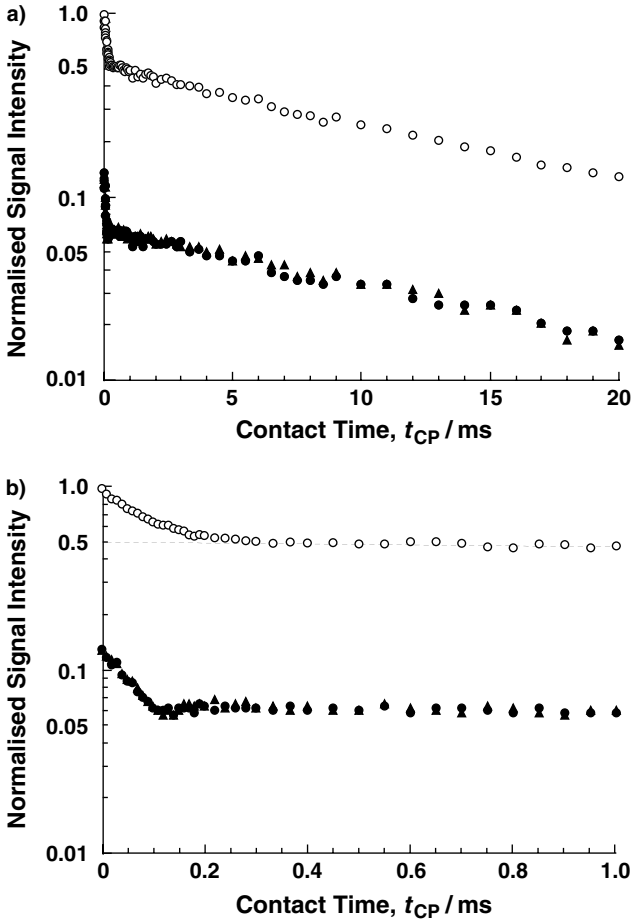

Figure 9. (a) Contact-time dependence of the ^{1}H signal intensity for the $^{1}H \rightarrow {}^{19}F$ CP-drain experiment on PVDF and (b) its magnification for short contact times to show the dipolar oscillation behaviour. The dipolar oscillation is observed only for the spinning sidebands.

very small (these assumptions should be valid for PVDF, in view of the large difference between T^{*}_{HF} and $T^{*}_{1\rho}$). The value of N_F/N_H thus calculated from the intercept (0.5) is 1.0, which is the same as the value expected from the chemical structure of PVDF. These facts indicate that the CP dynamics behaviour between ^{1}H and ^{19}F spins in PVDF can be acceptably explained in terms of the phenomenological spin thermodynamics theory[15,16] in spite of its two-phase (immobile and mobile) nature. In addition, pulse sequences using CP between the abundant proton and fluorine atoms, such as $^{1}H \rightarrow {}^{19}F$ CP, $^{1}H \rightarrow {}^{19}F$ IRCP, $^{1}H \rightarrow {}^{19}F$ CP-drain and $^{19}F \rightarrow {}^{1}H$ CP techniques, give complementary and consistent information concerning the CP behaviour in PVDF.

CONCLUSION

The solid-state $^{1}H \rightarrow {}^{19}F$ CP/MAS spectra of PVDF with ^{1}H decoupling can be fitted by five Lorentzian functions, and the spectrum of the amorphous domains containing regio-irregular structures was selectively observed by the DIVAM pulse sequence, which can be fitted by three Lorentzian functions. Significant differences in $T^{F}_{1\rho}$ and $T^{H}_{1\rho}$ between the

crystalline and amorphous domains were confirmed by spin-lock experiments in the ^{19}F channel under high-resolution conditions, in spite of the influence of spin diffusion from the crystalline to amorphous domain at longer spin-lock times. In addition, the effective time constants, T^*_{HF} and $T^*_{1\rho}$, determined from the $^1H \rightarrow {}^{19}F$ CP curves, are also significantly different between the two domains. The true values of T_{HF} are almost twice as large as the effective value of T^*_{HF}, which coincides well with the prediction of the theory. Dipolar oscillations were observed for the CP curves of the crystalline domain at short contact times. Such oscillations were not observed for the amorphous peak in the $^1H \rightarrow {}^{19}F$ CP experiment. On the other hand, dipolar oscillations were observed also for the amorphous peak in the $^1H \rightarrow {}^{19}F$ IRCP experiment but with a significantly lower frequency than for the crystalline domain. This difference is straightforwardly ascribed to motion of the polymer chain in the amorphous domain. In addition, the fact that the amorphous domain oscillation is also slower than that of the regio-irregular sequence indicates that the former undergoes more vigorous molecular motion than the latter, perhaps because the chain imperfections may be concentrated at crystalline/amorphous boundary regions. Although no spectral separation was obtained between the two domains in the $^{19}F \rightarrow {}^1H$ CP/MAS and $^1H \rightarrow {}^{19}F$ CP-drain MAS spectra, the results are consistent with the amorphous domain contributing to the main peak to a greater extent than to the sidebands. The main peak includes 55–60% of a short-decaying component, whose values of $T^F_{1\rho}$ and $T^H_{1\rho}$ are similar to those of the amorphous domain measured from the ^{19}F spectra. On the other hand, the sidebands in the ^1H spectra do not have such short-decaying components, and the values of $T^F_{1\rho}$ and $T^H_{1\rho}$ are similar to those of the long-decaying component of the main peak. In addition, these values are of the same order of magnitude as those of the crystalline domains measured from the ^{19}F spectra. The effective time constants, T^*_{FH}, T^*_{HF} and $T^*_{1\rho}$, determined from the $^{19}F \rightarrow {}^1H$ CP/MAS and $^1H \rightarrow {}^{19}F$ CP-drain MAS experiments, are consistent with those from the $^1H \rightarrow {}^{19}F$ CP/MAS experiment, and distinct dipolar oscillation was only observed for the spinning sidebands in the $^{19}F \rightarrow {}^1H$ CP/MAS spectrum. This indicates that ^{19}F magnetization rapidly transfers to the protons in the crystalline domain. The value of N_F/N_H calculated from the intercept of the CP-drain curve at $t_{CP} = 0$ (1.0) is consistent with that of the chemical structure of PVDF.

Acknowledgements

We thank the UK Engineering and Physical Sciences Research Council for research grant GR/M73514, which enabled the spectrometer to be purchased. One of us (S.A.) is grateful to the Japan Society for the Promotion of Science for a research fellowship held at Durham. We also appreciate research discussions with P. Holstein, A. M. Kenwright, B. J. Say, U. Scheler and J. Hirschinger. We thank a referee for pointing out an inconsistency in our original interpretation of oscillations in the CP curve.

REFERENCES

1. Nalwa HS. *J. Macromol. Sci., Rev. Macromol. Chem. Phys.* 1991; **C31**: 341.
2. Baltá Calleja FJ, González Arche A, Ezquerra TA, Santa Cruz C, Batallán F, Frick B, Lopez Cabarcos E. *Adv. Polym. Sci.* 1993; **108**: 1.
3. Ferguson RC, Brame EG. *J. Phys. Chem.* 1979; **83**: 1397.
4. Tonelli AE, Schilling FC, Cais RE. *Macromolecules* 1982; **15**: 849.
5. Cais RE, Kometani JM. *Macromolecules* 1985; **18**: 1357.
6. Lin F, Lin F. *J. Macromol. Sci. Chem.* 1989; **A26**: 1.
7. Katoh E, Ogura K, Ando I. *Polym. J.* 1994; **26**: 1352.
8. Holstein P, Harris RK, Say BJ. *Solid State Nucl. Magn. Reson.* 1997; **8**: 201.
9. Scheler U, Harris RK. *Solid State Nucl. Magn. Reson.* 1996; **7**: 11.
10. Holstein P, Scheler U, Harris RK. *Polymer* 1998; **39**: 4937.
11. Holstein P, Scheler U, Harris RK. *Magn. Reson. Chem.* 1997; **35**: 647.
12. Scheler U. *Bull. Magn. Reson.* 1999; **19**: 52.
13 Su TW, Tzou DLM. *Polymer* 2000; **41**: 7289.
14. Ando S, Harris RK, Holstein P, Reinsberg SA, Yamauchi K. *Polymer* 2001; **42**: 8137.
15. Ando S, Harris RK, Reinsberg SA. *J. Magn. Reson.* 1999; **141**: 91.
16. Ando S, Harris RK, Monti GA, Reinsberg SA. *Magn. Reson. Chem.* 1999; **37**: 709.
17. Aliev AE, Harris KDM. *Magn. Reson. Chem.* 1994; **32**: 366.
18. Zumbulyadis N. *J. Chem. Phys.* 1987; **86**: 1162.
19. Holstein P, Monti GA, Harris RK. *Phys. Chem. Chem. Phys.* 1999; **1**: 3549.
20. Teyssedre G, Bernes A, Lacabanne C. *J. Thermal Anal.* 1993; **40**: 711.
21. Brandrup J, Immergut EH, Grulke EA (eds). *Polymer Handbook* 4th edn. John Wiley & Sons: New York, 1999; chapt. 6.
22. Tonelli AE, Schilling FC, Cais RE. *Macromolecules* 1981; **14**: 560.
23. Lando JB, Hanes MD. *Macromolecules* 1995; **28**: 1142.
24. Müller L, Kumar A, Baumann T, Ernst RR. *Phys. Rev. Lett.* 1974; **32**: 1402.
25. Naito A, McDowell CA. *J. Chem. Phys.* 1986; **84**: 4181.
26. Ando S, Harris RK, Hirschinger J, Reinsberg SA, Scheler U. *Macromolecules* 2001; **34**: 66.
27. Reinsberg SA, Ando S, Harris RK. *Polymer* 2000; **41**: 3729.
28. Filip C, Hafner S, Schnell I, Demco DE, Spiess HW. *J. Chem. Phys.* 1999; **110**: 423.